

Detailed investigation of absorption, emission and gain in Yb:YLF in the 78–300 K range

UMIT DEMIRBAS,^{1,2,*}  JELTO THESINGA,¹ MARTIN KELLERT,¹
FRANZ X. KÄRTNER,^{1,3}  AND MIKHAIL PERGAMENT¹

¹Center for Free-Electron Laser Science, Deutsches Elektronen-Synchrotron DESY, Luruper Chaussee 149, 22761 Hamburg, Germany

²Laser Technology Laboratory, Antalya Bilim University, 07190 Dosemealti, Antalya, Turkey

³Physis Department and The Hamburg Centre for Ultrafast Imaging, University of Hamburg, Luruper Chaussee 149, 22761 Hamburg, Germany

*uemit.demirbas@cfel.de

Abstract: We present spectroscopic measurements focusing on a detailed investigation of temperature dependence of absorption, emission and gain in the uniaxial Yb:YLF laser gain medium. Measurements are carried out in the 78–300 K range, but we especially targeted our attention to the 78–150 K interval, which is the desired working range of liquid nitrogen cooled cryogenic Yb:YLF lasers/amplifiers. A tunable (770–1110 nm) Cr:LiSAF laser with around 100 mW continuous-wave output power and sub-0.2 nm bandwidth is used as an excitation source. The average power of the Cr:LiSAF laser is low enough to prevent heating of the sample, and its spectral flux (W/nm) is high enough to enable large signal-to-noise ratio measurements. Measured absorption data is used to cross-check the validity of the emission measurements, while the measured temperature dependent small-signal gain profile provided a second independent confirmation. The acquired absorption cross section curves match the previous literature quite well, whereas the measured strength of c-axis emission is stronger than some of the earlier reports. Direct measurements of small signal gain confirmed the emission cross section data, where single pass gain values above 50 have been measured for the 995 nm transition of E//c axis at 78 K. We further provide simple analytic formulas for the measured temperature dependence of absorption and emission cross section. We hope the presented results to be useful for the development of next generation of cryogenic Yb:YLF laser and amplifier systems.

© 2021 Optical Society of America under the terms of the [OSA Open Access Publishing Agreement](#)

1. Introduction

High-average and peak power laser and amplifier systems based on ytterbium-doped gain media are interesting tools for many applications including nonlinear pulse compression [1], optical parametric chirped-pulse amplification [2], parametric-waveform synthesis [3], and table-top electron acceleration [4]. With its thermo-opto-mechanical strength, Yb:YAG gain media become the working horse of such applications [5–10]. However, the relatively narrow gain profile of Yb:YAG results in pulsewidths longer than 500-fs at room temperature, which even prolongs to few picoseconds at cryogenic temperatures [11].

Yb:YLF (Yb:LiYF₄) is an interesting alternative material with broad bandwidths that could ideally support 100-fs level pulses both at room and cryogenic temperatures [12–29]. Nevertheless, compared to Yb:YAG, Yb:YLF is not yet well studied and many of its thermo-opto-mechanical parameters are not well known, or their temperature dependence is not well investigated. For a successful design of a laser/amplifier system, one of the first parameters a laser scientist needs to know in detail is the absorption, emission and gain profile of the laser medium at different temperatures. For cryogenic Yb:YLF laser/amplifier system, our recent experimental work has shown that, during laser operation the average temperature of the liquid nitrogen cooled Yb:YLF crystal varies in the ~80–150 K range depending on the thermal load on the crystal [30]. However,

in our design/simulation attempts [31], we have realized that, the literature lacks temperature dependence of data even in these basic parameters (absorption, emission and gain): (i) data is plotted in small graphs with limited spatial resolution, (ii) the data is taken with low spectral resolution, (iii) the data is only given for a few selected temperatures, (iv) the data is only given in arbitrary units, and (v) sometimes the data available from variable sources conflict with each other. Unfortunately, due to the exponential nature of the amplification process (e.g. in a regen one can easily have >100 round trips), even small uncertainties in laser parameters could result in significantly different performance estimate. Hence, it is important to investigate the temperature variation of absorption, emission and gain in Yb:YLF carefully (especially in the 78–150 K range [30]), for the successful development of next generation of cryogenic Yb:YLF laser and amplifier systems which could potentially reach kW level average powers along with pulsedwidths in the sub-250-fs range. Such spectroscopic information could also be useful for the optical refrigeration community (that partially base their efforts on anti-Stokes emission of Yb:YLF crystals) [32–38], in their attempts to develop nanometer scale quantum optical devices [36].

Motivated by this need, we have focused our attention on careful measurement of temperature dependence of absorption, emission and gain in Yb:YLF. As the main tool, we have used a home-build continuous-wave Cr:LiSAF laser, that could be tuned from 770 nm to 1110 nm [39–41]: a span that covers both the absorption and emission range of Yb:YLF gain media. The experiments involved careful measurement of absorption and gain in Yb:YLF at different temperatures while using a tunable Cr:LiSAF laser as an excitation/seed source. We have further measured emission spectrum of Yb:YLF, and calculated the emission cross section (ECS) spectra using the Füchtbauer-Ladenburg relation [42–44].

To our knowledge, we present here the first set of measurements on polarization, temperature and wavelength dependence of gain in Yb:YLF. Furthermore, along with a few other studies, this is the first detailed report on temperature dependence of absorption and emission in Yb:YLF. We also provide simple analytic formulas for the modelling of measured temperature dependence of absorption and emission, as it is usually very hard to get quantitative information from the published data.

The measured absorption cross section (ACS) curves in this study match the previous literature quite well and considerably extend the available temperature dependent data. Our emission cross section (ECS) measurements underline a stronger c-axis emission than what is reported in some of the earlier work, and complements the literature with detailed analysis. The observed discrepancy in ECS results motivated us to implement a two-step verification approach for the validation of our results. As the first approach, we have compared the emission measurement results with the independently taken ACS data via the McCumber relation [45–48]. As the second step, ECS data is used to calculate gain cross section (GCS) spectra, which is then cross-checked via direct small signal gain measurements. Both schemes produced results that confirm each other quite well, as it will be outlined in detail through the manuscript.

The paper is organized as follows: In Section 2, we summarize the experimental setup and the methodology that is employed. In Section 3, we start with presentation of absorption measurements. Section 4 presents the emission cross section measurement in great detail. In Section 5, we use the McCumber theory to validate our ECS measurements by comparison of absorption and emission data. In Section 6, we estimate gain profiles at different temperatures using the measured emission data, whereas in Section 7 we cross-check our results one more time by direct measurement of small signal gain. Finally, in Section 8, we close with a brief discussion.

2. Experimental methodology

Figure 1 provides a sketch of the experimental setups used in this study for the emission, absorption and gain measurements. A 675 nm tapered-diode laser (TDL) [49,50] pumped continuous-wave

(cw) Cr:LiSAF laser (Fig. 1(a)) was used in the spectroscopy experiments [39–41]. A 3-mm-thick crystal quartz birefringent filter (BRF) with an optical axis 45° to the surface of the plate was used to tune the laser wavelength [51]. The BRF was inserted at Brewsters angle into the laser resonator near the cavity high reflector mirror. The free spectral range of the plate is greater than 350 nm, preventing wavelength jumps and instabilities. Via simple rotation of the BRF plate, the Cr:LiSAF laser provided broadly tunable cw output with up to 100 mW of output power in the 770–1110 nm range (usage of two different output couplers was required to cover the whole range) [52]. The spectral width of the Cr:LiSAF laser output was narrower than 0.2 nm (FWHM: full-width at half-maximum) in the whole tuning range (was below 0.05 nm in most of the range). Compared to setups that use lamp sources, the usage of Cr:LiSAF laser enables a relatively high spectral flux (W/nm). Combined with a diffraction limited beam profile this enables measurements with large signal-to-noise ratio. During the measurements, the Cr:LiSAF laser output is collimated using a 100 mm lens, and the beam diameter on the sample was around 1.35 mm for absorption and gain measurements. A smaller beam size of around 100 μm is used for the emission measurements to minimize self-absorption effects (the excited volume is smaller, and the fluorescence collected transverses a smaller path to reach the detector, which helps to minimize radiation trapping).

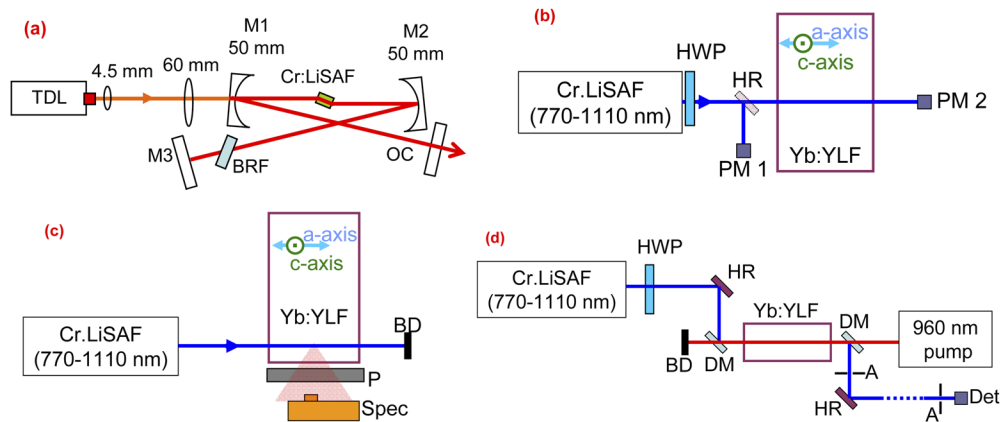


Fig. 1. A simplified schematic of the setups used in spectroscopy experiments: (a) A simple schematic of tapered-diode laser (TDL) pumped cw Cr:LiSAF laser with broad tunability (770–1110 nm) that is used as the seed/excitation source, (b) Absorption measurement system (HR mirror is on a flip mount), (c) Fluorescence emission measurement system and (d) Small-signal gain measurement setup. The Yb:YLF crystal that is mostly used in measurements was an a-cut sample, with the axes oriented as shown. The dashed line in (d) indicates a relatively long distance, which is used to minimize ASE on the detector. M1-M3: Cr:LiSAF laser cavity dichroic and high reflector mirrors, OC: Output coupler, BRF: birefringent tuning filter, HR: High reflector, PM1-PM2: Sensitive power meters, P: Film polarizer, Spec: Spectrometer used for measuring the emission spectrum, BD: beam dump, HWP: Half-wave plate, DM: Dichroic mirror, A: Aperture, Det: Detector used in gain measurements.

Several a-cut and c-cut Yb:YLF crystals with 1% Yb-doping and 2 cm length were available for the experiments. The crystals were indium soldered from the top side to a multi-stage pyramidal cold head, which was cooled to cryogenic temperatures by boiling liquid nitrogen using a vacuum sealed dewar system. Silicon based thermal sensors connected to the cold head near the crystal enabled real time measurement of cold head temperature with ± 0.1 K accuracy. For temperature dependent measurements, we have used the slow cooling cycle of the dewar (that typical took

6–7 hours) [53]. Care is taken during the measurements not to heat up the crystal by minimizing the power of the excitation beam as well as the excitation duration.

For the absorption measurements a very simple setup is used as it is shown in Fig. 1(b). The Cr:LiSAF output beam (diameter: 1.3 mm) is sent through the center of the Yb:YLF sample. The incident (I_i) and transmitted power (I_t) levels were measured carefully using a sensitive silicon photodiode power meter (Thorlabs S121C, resolution: 10 nW). The absorption of Yb:YLF crystal at each wavelength is calculated after subtracting the background loss of the system which includes small residual losses from the AR coatings of Yb:YLF crystal surface, and dewar windows. The sensitivity of the absorption measurements is limited by the intensity fluctuations of the Cr:LiSAF laser as well as by the accuracy of determining the background losses, which could be time dependent due to possible water condensation on the dewar inner windows or crystal surfaces (an almost leak free home/made dewar with a pressure better than 10^{-8} mbar at 78 K is used to minimize such effects). At the same time, the relatively narrow linewidth of the Cr:LiSAF laser (which stayed below 0.05 nm in most of the tuning range) is adequate to resolve many of the peaks at most of the temperatures.

Once the transmission (T) or absorption ($A=1-T$) of the sample is estimated at a specific wavelength and temperature, we have calculated the corresponding absorption cross section value ($\sigma_a(\lambda, T)$) using:

$$\sigma_a(\lambda, T) = -\frac{\ln(T)}{d N_{Yb}} \quad (1)$$

where \ln is the natural logarithm function, d is the thickness of the sample (20 mm in our case), and N_{Yb} is the density of active Yb ions (1.4×10^{20} ions/cm³ for the 1% Yb-doped YLF [18]). As mentioned earlier, if the absorption is known, and if the details of the energy levels creating the transition is known, McCumber relation could be used to estimate emission cross section from absorption cross section (or vice versa) using [45–48]:

$$\sigma_e(\lambda, T) = \frac{Z_l}{Z_u} \sigma_a(\lambda, T) \exp\left(\frac{E_{zl} - \frac{hc}{\lambda}}{kT}\right) \quad (2)$$

where h is the Planck constant, k is the Boltzmann constant, c is the speed of light in vacuum, E_{zl} is the energy of the zero phonon line transition, Z_u (Z_l) is the partition function of the upper (lower) laser manifold, and their ratio could be calculated using [54]:

$$\frac{Z_l}{Z_u}(T) = \frac{\sum_i \exp\left(-\frac{E_{li}-E_{l1}}{kT}\right)}{\sum_i \exp\left(-\frac{E_{hi}-E_{h1}}{kT}\right)} = \frac{1 + \exp\left(-\frac{E_{l2}-E_{l1}}{kT}\right) + \exp\left(-\frac{E_{l3}-E_{l1}}{kT}\right) + \exp\left(-\frac{E_{l4}-E_{l1}}{kT}\right)}{1 + \exp\left(-\frac{E_{h2}-E_{h1}}{kT}\right) + \exp\left(-\frac{E_{h3}-E_{h1}}{kT}\right)}. \quad (3)$$

Here E_{hi} (E_{li}) are the corresponding individual intra-manifold energies of the higher (lower) lying laser levels. There are some minor differences in the reported values of energy levels for Yb:YLF in literature [55–57], which might cause observable differences in the calculated ECS/ACS values due to the existence of exponentials in the McCumber relation (both in Eq. (2) and (3)). Here we have used the more recently reported values in [55]: $E_{l1} = 0$ cm⁻¹, $E_{l2} = 218$ cm⁻¹, $E_{l3} = 248$ cm⁻¹, $E_{l4} = 486$ cm⁻¹, $E_{h1} = 10293$ cm⁻¹, $E_{h2} = 10416$ cm⁻¹, $E_{h3} = 10554$ cm⁻¹. The corresponding wavelength for the zero-phonon line energy ($E_{zl} = 10293$ cm⁻¹) is around 971.53 nm (an assignment made at 12 K [55]). In our measurements, we have positioned this transition at 971.7 ± 0.25 nm at 78 K and 972 ± 0.25 nm at 200 K, respectively. We have used Eq. (2) to transfer knowledge from ACS to ECS, and vice versa, to confirm and cross-check our measurements.

The fluorescence emission spectra were measured at a 90° angle to the Cr:LiSAF beam propagation direction using a window at the side of the dewar (Fig. 1(c)). A thin film polarizer (Thorlabs LPNIRE100-B) was used for selecting the fluorescence emission in the relevant

axis. In the first set of experiments, we have checked the excitation wavelength dependence of fluorescence spectra and we have observed that the fluorescence spectral shape does not change for pump wavelengths in the 900–1020 nm range (some materials like Alexandrite might show different emission spectra when excited at different wavelengths [58]). As a result, we have chosen to use around 20 mW of 930 nm Cr:LiSAF light in the fluorescence emission measurements, a wavelength on the shorter wavelength side of emission, which enabled easy separation of background pump signal. A 3648 pixel CCD array (Toshiba TCD1304AP) based Ocean Optics spectrometer was used for recording the fluorescence spectra. The spectrometer had a spectral resolution of 0.1 nm in the 900–1060 nm range (spectrometer recorded 3600 data points with an average wavelength separation of ~0.05 nm). The calibration of the spectrometer (estimated to be better than ± 0.25 nm) was first confirmed using Ar and Kr lamp lines. The overall spectral response of the measurement system was corrected using the known spectral response curves and a fluorescence intensity accuracy better than $\pm 20\%$ is estimated for the 900–1025 nm range (the sharp drop of Si CCD array sensitivity creates higher uncertainty for wavelengths above 1025 nm). Note that care is taken to minimize self-absorption effects, which is known to produce errors in emission spectrum measurements in Yb-based systems. For that, a relatively lowly Yb-doped (1%) sample is used, and the Yb:YLF crystal is excited from its edge using a relatively small (100 μm) excitation beam. Furthermore, we have also corrected the spectra for self-absorption losses, similar to what is employed in [59], by calculating the self-absorption losses of the emission beam that reaches to the spectrometer (absorption of ~2 mm of 1% Yb-doped material is considered). Note that, despite the care, as it will be discussed in detail later, we have still observed some self-absorption induced small errors in emission spectra especially for measurements near room-temperature: lower ECS strength is measured at shorter wavelengths due self-absorption. On the other hand, since the overlap of absorption and emission bands decrease with decreasing temperatures, errors due to self-absorption effect were minimal in the 78–150 K range, which is the main region of interest for the cryogenic laser/amplifier systems. This issue will be discussed in more detail while presenting the experimentally measured values.

The normalized emission cross section ($\sigma_e(\lambda)$) curves are obtained by multiplying the measured fluorescence emission spectrum by a factor of λ^5 (where λ is the emission wavelength) [42,53], and then renormalizing the curves. The emission cross section in absolute units is calculated using the modified Füchtbauer–Ladenburg formula [42–44]:

$$\sigma_{e,a}(\lambda, T) = \frac{\lambda^5}{8\pi cn^2 \tau_R} \frac{I_a(\lambda)}{\int \left(\frac{1}{3} I_c(\lambda) + \frac{2}{3} I_a(\lambda) \right) \lambda d\lambda} \quad (4)$$

$$\sigma_{e,c}(\lambda, T) = \frac{\lambda^5}{8\pi cn^2 \tau_R} \frac{I_c(\lambda)}{\int \left(\frac{1}{3} I_c(\lambda) + \frac{2}{3} I_a(\lambda) \right) \lambda d\lambda} \quad (5)$$

where $I_{a,c}(\lambda)$ are the measured emission intensities in the a, c axis of the uniaxial crystal, n is the average refractive index of gain medium (~1.46 [60] around 1 μm in YLF), τ_R is the radiative lifetime of the upper laser level ($^2F_{5/2}$) involved in transition. For Yb:YLF, due to the presence of radiation trapping (on top of possible non-radiative effects), it is difficult to accurately measure radiative lifetime. One alternative solution is to obtain emission cross section values from the measured absorption data using McCumber relation (Eq. (3)), and calculate the radiative lifetime using Füchtbauer–Ladenburg formula given above. This approach yielded a value of $\sim 2040 \pm 180$ μs in a recent study [47] (a value of 2270 μs is found in an earlier study [48]). In our work, for the 1% Yb-doped YLF sample, we have measured fluorescence lifetimes of 1970 ± 50 μs at 78 K and 2120 ± 50 μs at 300 K, in a setup which we tried to reduce the radiation trapping effects [61]. We believe that, the slightly longer fluorescence lifetime we measured at 300 K still might be due to the radiation trapping effect which is hard to completely eliminate at room-temperature.

Overall, we have chosen to use a radiative lifetime value of 2000 μs in this study. We would like to also mention here that, after repeating the temperature dependent measurement required for ECS determination 3–4 times, we have seen that, despite ultimate care in the fluoresce collecting and measurement process, due to alignment sensitivities, it is very challenging to make accurate absolute measurements of $I_a(\lambda)$ and $I_c(\lambda)$. As discussed in detail in [47], we have perfected our alignment process to the best of our abilities (confirmed the setup with the homogeneous Yb:YAG crystal), and also used the measured temperature dependent absorption data and McCumber relation to reduce the uncertainties in our ECS calculations (by cross-checking the ECS and ACS data with each other).

The setup that is used for the gain measurements is shown in Fig. 1(d). In the setup, the weak Cr:LiSAF beam plays the role of a low power seed beam, which we use to measure small signal gain. Two 2 inch size 45° dichroic mirrors were used to couple in and out the 960 nm high power pump source that is used for the main excitation of Yb:YLF crystal. The 960 nm pump diode had an M^2 of around 220 and was focused to a spot diameter of 3.2 mm inside the gain media. The smaller Cr:LiSAF beam (1.3 mm) pass through the central region of the excitation area and observes an almost flat-top excitation profile. In small signal gain measurements of the E//a axis, the gain medium is excited with 2 ms long pump pulses with 2 kW of peak power at 0.1 Hz repetition rate. Due to the low duty cycle employed, the average absorbed pump power was below 0.5 W in these measurements, and hence the heat load on the crystal is quite limited (we estimate an average temperature rise below 0.1 K at this average pump power [30], whereas instant peak temperatures might be 2–3 K higher). For the gain measurements in E//c axis, the pump pulse duration is reduced from 2 ms to 250 μs to minimize amplified spontaneous emission (ASE) effects observed in this higher gain emission band. Note that, to minimize the role of ASE in gain measurements, we have put two small circular apertures and propagated the amplified Cr:LiSAF beam 2–3 meters (ASE component is reduced by spatial filtering). Furthermore, a background signal is also taken (while seeding the system above 1050 nm, a region outside of gain bandwidth) and this small background is reduced from the measurements. The Cr:LiSAF beam power is recorded again with the sensitive silicon photodiode power meter (Thorlabs S121C sensor in the PM100A power meter), and the analog output of the power meter with sub-1- μs response time was monitored by a fast 500 MHz oscilloscope and simultaneously recorded by the computer for gain calculations. The measured small signal gain values are the maximum gain values of the system that is acquired just after the tail of the 960 nm pump.

To enable a further independent cross-check of ACS/ECS results, we have compared the measured small signal gain spectra at 78 K and 295 K, with the gain spectrum estimated from earlier emission and absorption measurements. The effective gain cross section (GCS) spectra ($\sigma_g(\lambda, T)$) of Yb:YLF is estimated using:

$$\sigma_g(\lambda, T) = \beta\sigma_e(\lambda, T) - (1 - \beta)\sigma_a(\lambda, T) \quad (6)$$

where β is the fractional population inversion level and all the other parameters are as defined above. The small signal gain coefficient (g_0) could be calculated from $\sigma_g(\lambda, T)$ using:

$$g_0(\lambda, T) = \sigma_g(\lambda, T)N_{Yb} \quad (7)$$

where N_{Yb} is the number density of the active Yb^{3+} ions in the YLF sample. Note that single pass fractional gain $\text{Exp}(g_0d)$ could be then easily estimated (d : length of the gain medium). As a side note, for a long gain sample such as ours, the inversion will strongly vary with position: will be higher at the front of the crystal where most of the absorption happens and will then decay towards the end of the crystal (the exact profile will depend on incident pump power, pump spot size, pump spectral width, absorption saturation effects, etc. . .). Hence, position dependence should also be included in the above discussion for an accurate calculation of Yb:YLF gain.

3. Absorption measurements

We start presentation of our experimental results with Fig. 2(a-b), which shows the measured absorption of the 1% Yb-doped 2 cm long YLF sample at 78 K and 300 K, for both E//a and E//c axis, respectively. The corresponding absorption cross section values are then shown in Fig. 2(c-d), where we have used the known doping and thickness of the sample for the calculation. Note that, to enable better visibility a second axis is used to show the ACS values at room temperature. Moreover, a 5-times vertically expanded version of the 78 K ACS curve is also shown to enable a zoom in view to the details of the measurement.

The measured room-temperature absorption profile matches very well (difference smaller than $\pm 5\%$) to the measurement presented in [18] for a 5% Yb-doped YLF sample, and is also in relatively good agreement with other measurements in literature [21,47,48,55,59,63–65]. Note that the scale of ACS graphs for RT emission is different for the different polarizations, and the absorption strength in E//c axis is stronger compared to E//a axis. To our knowledge, Fig. 2 contains the first detailed cryogenic absorption measurement of Yb:YLF for wavelengths longer than 975 nm: knowledge of absorption in this region is important in determination of quasi-3-level operation parameters of Yb:YLF laser systems [10].

As outlined in [55], due to strong electron-phonon coupling, it is difficult to identify origins of the absorption lines of Yb especially at room-temperature, and different absorption peaks appear for different polarizations. Here, in Fig. 2(e), we also provide the energy level diagram of Yb:YLF, where the data on intra-manifold energies of the Stark levels are taken from [55]. Note that, we have also included calculated wavelengths for transitions and Boltzmann occupancy factors for the different Stark levels at selected temperatures of 78 K, 150 K and 300 K [62]. Note that origins of some of the absorption peaks can be easily understand by looking at the possible transitions in Fig. 2(e). On the other hand, some transitions, like the absorption peak around 935 nm is believed to be a vibronic side-peak induced by strong electron-phonon coupling [55]. We refer the reader to Ref. [55] for a more detailed discussion on origins of transitions observed in the measured absorption.

For cryogenic lasing/amplifier applications the ACS at 78 K is more interesting, and we see that, as the phonon energies decrease with decreasing temperature, due to reduced electron-phonon coupling effects, the transitions get stronger and narrower. The measured ACS spectrum at 78 K matches relatively well to most of the previously reported measurements in literature [47,59,62], except small minor differences on peak values, which might be due to the limited resolution and dynamic range of different measurement systems. As an example, we have measured a peak absorption value of $5.6 \times 10^{-20} \text{ cm}^2$ for the 960.35 nm transition of E//c absorption, where peak values of $\sim 5.9 \times 10^{-20} \text{ cm}^2$ [25], $\sim 5 \times 10^{-20} \text{ cm}^2$ [62], and $6.5 \times 10^{-20} \text{ cm}^2$ [59] are reported in earlier work. Similarly, for the same peak, we have measured a value of $2.5 \times 10^{-20} \text{ cm}^2$ for the E//a axis, that is in relatively good agreement with $2.7 \times 10^{-20} \text{ cm}^2$ of [62], $\sim 2 \times 10^{-20} \text{ cm}^2$ of [25], and $\sim 2.4 \times 10^{-20} \text{ cm}^2$ of [59]. As a side note: (i) our measurements differ from what is reported in [17,47], (ii) further cryogenic absorption data for Yb:YLF is also available in [56] (15–300 K in arbitrary units), and in [21,55,64] (at 15 K, for un-polarized light).

The difference of 78 K absorption between the E//a and E//c axis is also noteworthy. First of all, the E//a absorption is broader and enables efficient pumping around 934 nm, 948 nm and 960 nm. Note that, the 934 nm and 948 nm absorption transitions are rather weak in the E//c axis absorption. As mentioned above, the 960 nm transition with a FWHM of ~ 2 nm is strong for both axes (stronger in E//c) and enables efficient pumping of cryogenic Yb:YLF laser systems [26,27,29]. The strong zero-phonon absorption line around 971.7 nm could ideally enable pumping with a lower quantum defect, which has a measured value of $\sim 4 \times 10^{-20} \text{ cm}^2$ and $\sim 1.8 \times 10^{-20} \text{ cm}^2$, for the E//a and E//c axis, respectively. On the one hand, this line is too sharp for high-power diode pumping at 78 K. On the other hand, under thermal load, the Yb:YLF crystal could easily reach 125–175 K temperatures, and the linewidth of the 971.7 nm line at

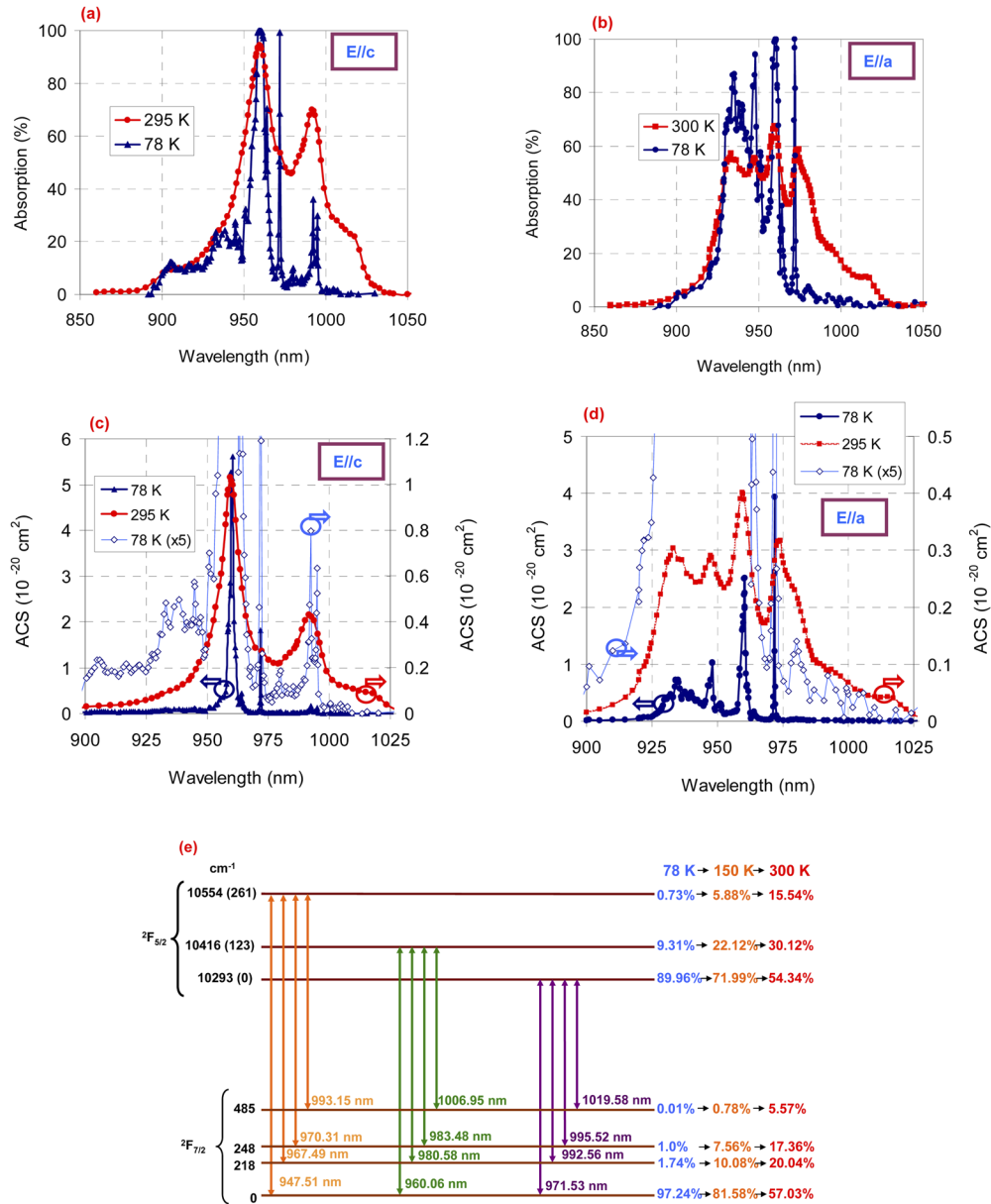


Fig. 2. Measured room-temperature (295 K) and 78 K absorption spectra of 2 cm long 1% Yb-doped YLF crystal in (a) E//c and (b) E//a axes. Corresponding calculated absorption cross section (ACS) spectra is shown in (c) and (d). The secondary vertical axes in (c-d) show the ACS cross section at RT, as well as 5-fold multiplied 78 K curve for better visibility. An energy level diagram of Yb:YLF is shown in (e), along with the calculated Boltzmann occupancy percentages of Stark levels at 78 K, 150 K and 300 K, respectively [55,62].

these temperatures (~ 0.5 – 1 nm) might be sufficient enough for the utilization of this pumping scheme.

As discussed earlier, our absorption measurements are taken using the Cr:LiSAF laser, where measurement of absorption spectra at each temperature requires tuning of the Cr:LiSAF laser wavelength to the desired point and measuring incident and transmitted powers, and the overall process takes time. As a result, we have only measured absorption spectra of Yb:YLF at 78 K and 295 K. However, we have measured variation of absorption with temperature at selected wavelengths using the cooling cycle of the dewar, and the results are summarized in Fig. 3. Note that, the measured variation of absorption at the pump wavelength region (960.4 nm and 971.7 nm) contains important information on the variation of pump absorption with temperature, whereas the measured variation of absorption at the lasing wavelength region (above 990 nm) provides important information for the amount of self-absorption losses.

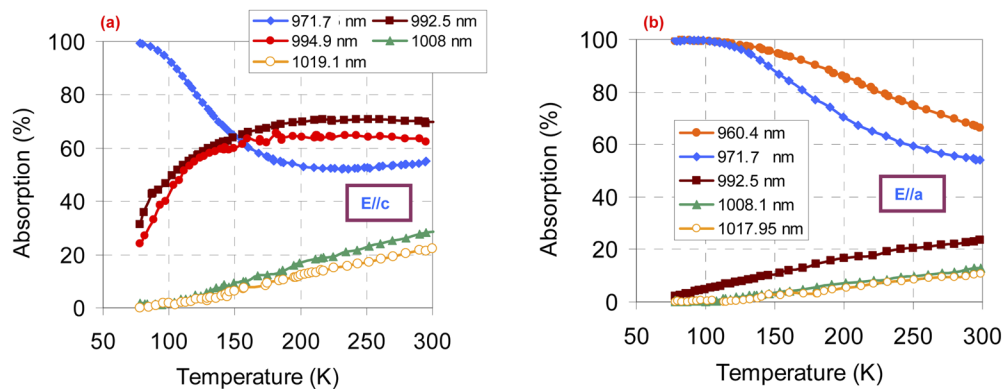


Fig. 3. Measured variation of absorption of Yb:YLF crystal with temperature in the 78–300 K range, at selected wavelengths for (a) E//c and (b) E//a axes. A 1% Yb-doped 2 cm long YLF crystal was used in the measurements.

It is educational to try to roughly understand the trends observed in Fig. 3. For that, we can use the energy level diagram that is shown earlier in Fig. 2(e). As an example, for wavelengths at the far edge of absorption (above 995 nm), the absorption originates mostly from the highest lying Stark level of the $^2F_{7/2}$ manifold. At 78 K, this Stark level is mostly empty (posses 0.1% of the ions), and as one heats up the crystal this level slowly starts to fill up: 0.78% and 5.57% occupancy at 150 K and 300 K, respectively. As a result, for wavelengths such as 1008 nm, 1018–1019 nm, the measured absorption is very low at 78 K, but it starts to slowly increase with temperature as the population of the highest lying Stark level of the $^2F_{7/2}$ manifold increases. As another example, around 960 nm the absorption is due to the transition from the lowest lying Stark level of the $^2F_{7/2}$ manifold. The estimated Boltzmann occupancy factor for this level decreases from around 97.24% to 57.03% as the temperature is increased from 78 K to 300 K. As a result, the measured absorption for this band decreases with temperature due to the phonon broadening of the transition. As the last example we can look at the absorption near the zero phonon line around 971.7 nm, where again the absorption is believed to originate from the lowest lying Stark level of the $^2F_{7/2}$ manifold. Similar to the 960 nm transition, the absorption at this wavelength steadily decreases with temperature for the E//a axis. On the other hand, for the E//c axis, the absorption first decreases then saturates and then even start to increase with temperature. This shows that, as discussed in [55], even in a simple looking system like Yb:YLF, where one has only two energy manifolds, due to strong electron-phonon coupling, it is not always easy to interpret the measured trends in absorption. We will continue on this discussion in Section

5, where we will use the McCumber theory to calculate absorption spectra from the measured emission profile at different temperatures.

4. Emission cross section measurements

Figure 4 shows the measured variation of normalized emission cross section with temperature for the (a) E//c and (b) E//a axes, respectively. The peak of the emission in E//c axis is around 995 nm. For the E//a axis, the peak of the emission is around ~971.7 nm at 78 K, but we have chosen to normalize the spectra with respect to main emission band around 1016 nm. It is clear that, as the temperature increases the emission peaks get broader and smoother. As an interesting point, it is already noticeable that, the E//a emission band centered around 1016 nm possesses a broad bandwidth even at cryogenic temperatures, which we will elaborate in greater detail soon.

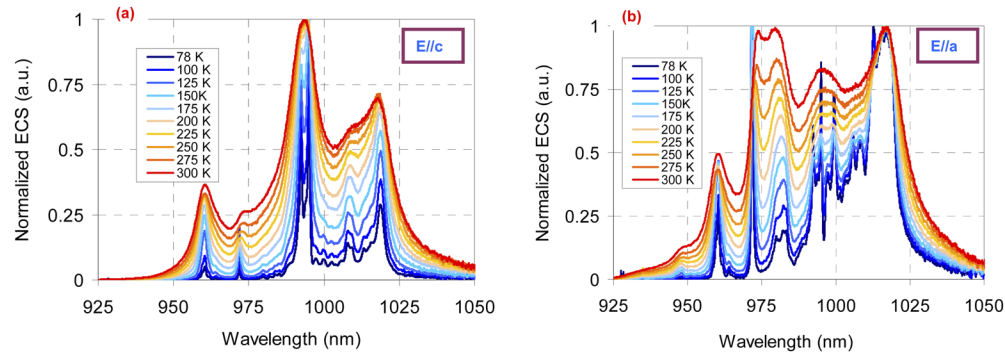


Fig. 4. Variation of normalized emission cross section (ECS) spectra of Yb:YLF with temperature for (a) E//c and (b) E//a axes at crystal temperatures ranging from 78 K to 300 K.

Emission data in normalized or arbitrary units are useful to understand how the shape of the emission bands change with temperature and polarization, and could be used in determining effects such as gain narrowing. On the other hand, knowledge of ECS in absolute/qualitative units gives more complete information, since the strength of the emission could also be acquired. For that purpose, in Fig. 5, we present our temperature dependent ECS measurement results of Yb:YLF for different polarizations. The same data is presented in two different vertical axis scales, for better readability of the small details.

At this point, it is educational to first carefully compare the measurements in this study with previous data in literature. To our knowledge, there are only a few earlier reports of temperature dependent emission for Yb:YLF: (i) Kawanaka et al.: ECS measurements at 77 K and 293 K [17], (ii) Bensalah et al.: ECS data at 12 K and 300 K [21,55,64], (iii) Sugiyama et al.: ECS measurement between 15 K and 300 K in arbitrary units [56], (iv) Fan et al.: ECS data at 80 K [25,59], (v) Selestskiy et al.: fluorescence measurement for E//c between 100 K and 300 K, in arbitrary units [66], (vi) Ter-Gabrielan et al.: ECS data at 77 K [62], and recently (vii) Korner et al.: ECS data between 80 K and 280 K [47]. First of all, when one looks at from a general perspective, we see that, the variation of spectral shape of the emission with temperature is rather similar in all studies, except a few work in which the resolution of the instrument created weaker lines with broader bandwidths and smoother emission profile. However, there are some observable differences in terms of absolute strength of the transitions especially for the E//c axis as we try to outline below.

For a more comprehensive comparison/investigation of the ECS data near the important laser bands, we have prepared Fig. 6, which shows the 1016 nm band of E//a axis, along with the ~995.2 nm and ~1019.5 nm transitions of the E//c axis in greater detail. Starting from the broadband E//a transition (Fig. 6(a)), we see that the transition has a FWHM bandwidth of

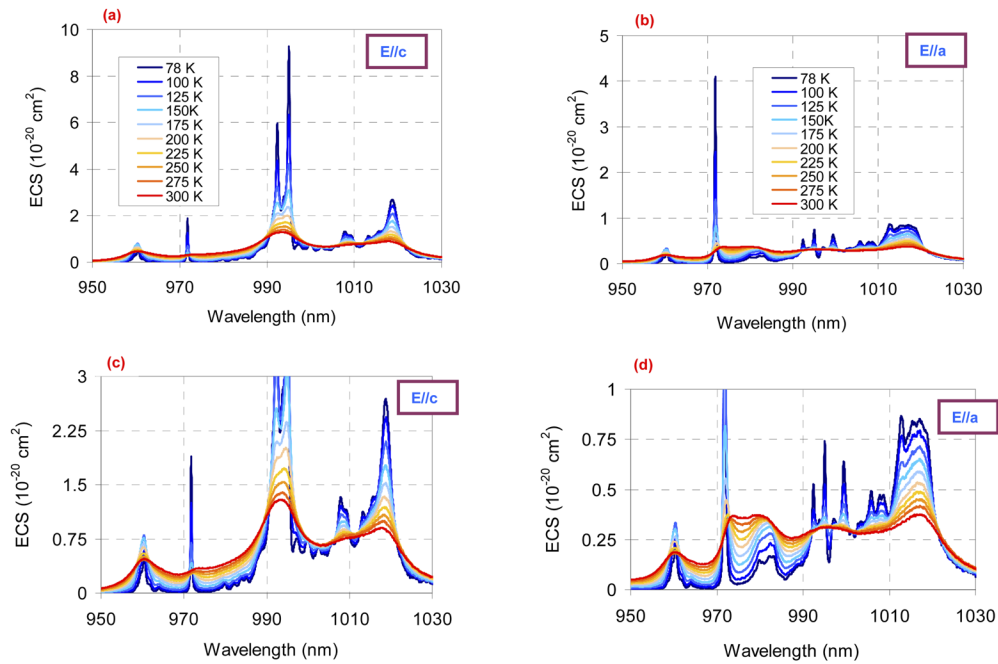


Fig. 5. Variation of emission cross section (ECS) spectra of Yb:YLF in absolute units with temperature for (a-c) E//c and (b-d) E//a axes of Yb:YLF at crystal temperatures ranging from 78 K to 300 K. In graphs (a-b) the whole spectra are shown, where as in graphs (c-d) we focus on weaker parts of the spectrum with lower ECS values.

around 9.7 nm at 78 K, which extends to a FWHM of 11 nm at 125 K, and gets even broader as the temperature increases. Due to the broad bandwidth of this transition, earlier Yb:YLF amplifier work has been mostly based on this emission [23,27,28,67]. At 78 K, the peak value of emission cross section in this transition is measured to be around $0.85 \times 10^{-20} \text{ cm}^2$, that is in good agreement with the values reported in literature ($\sim 1 \times 10^{-20} \text{ cm}^2$ [25,59], $\sim 0.75 \times 10^{-20} \text{ cm}^2$ [62], $\sim 0.88 \times 10^{-20} \text{ cm}^2$ [47]).

For the E//c axis, usually the sharp peak around 995 nm is employed in cryogenic lasing experiments due to much higher gain in this band [25,62]. We have measured a peak ECS value of $9.3 \times 10^{-20} \text{ cm}^2$ for the 995 nm line, which is in good agreement with the recent measurement ($9.4 \times 10^{-20} \text{ cm}^2$) by Korner et al [47], but rather higher than what is reported in other studies ($5.7 \times 10^{-20} \text{ cm}^2$ in [62] and $\sim 4 \times 10^{-20} \text{ cm}^2$ in [25,59]). Bensalah et al. measured a peak value of $\sim 12 \times 10^{-20} \text{ cm}^2$ for the E//c axis 995 nm transition at 12 K, which confirms the strength and sharpens of this peak at cryogenic temperatures [21,55,64], and support the relatively high 78 K value presented in this work. When we look at the broader 1019.5 nm transition of E//c axis, we find a FWHM value of 3.7 nm at 78 K, which extends to a FWHM of 6.5 nm at 125 K. The 1019.5 nm band of E//c axis is not as broad as the 1016 nm E//a band, but we have measured a peak value of $2.7 \times 10^{-20} \text{ cm}^2$ for the 1019.5 peak at 78 K, indicating presence of 2–3 fold higher gain in this band. The peak value we have measured at 1019.5 nm is slightly higher than earlier measurements in literature ($2 \times 10^{-20} \text{ cm}^2$ in [47], $1.8 \times 10^{-20} \text{ cm}^2$ in [25,59]). A peak ECS value of around $4 \times 10^{-20} \text{ cm}^2$ is reported at 12 K in [21,55,64], which again might be seen as a confirmation of the larger ECS value reported in our work. The recent detailed ECS results reported by Cante et al. for Yb:LLF [68], a crystal with quite similar spectroscopic behavior [21], also shows similar spectroscopic strength for E//c axis. The lower values reported in some of the earlier Yb:YLF studies might be due to the limited resolution of measurements or local

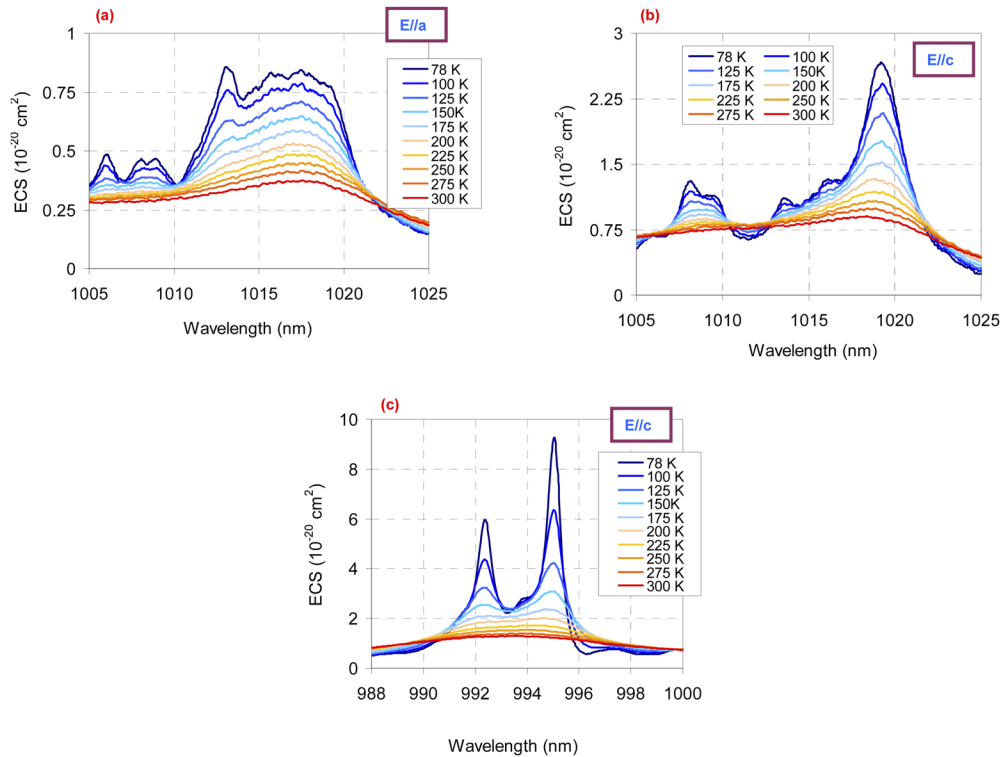


Fig. 6. Calculated variation of emission cross section (ECS) spectra of Yb:YLF with temperature around the main lasing bands for the (a) E//a and (b-c) E//c axes.

heating of the sample which could broaden and weaken the transition (even a few K could create a difference for some transitions).

As another note, when we look at the overall strength of the E//c and E//a axis (the integrated emission strength), we have measured a quite strong E//c axis in our measurements, with an integrated spectral intensity ~ 2 – 2.5 times higher than E//a axis (around 2 at room-temperature which increased monotonically to around 2.5 at 78 K). Looking at the literature, this observation is in good agreement with the spectra shown in [21,47,55,64], but some other studies report a slightly weaker E//c emission (~ 1.5 – 2 ratio rather than a ~ 2 – 2.5 ratio between E//c and E//a emission). Unfortunately, it is rather difficult to get absolute measurements of ECS, and slight differences in the measured ratio of different axis could also result in observed differences in reported ECS values. Hence, in the coming sections, the accuracy of our ECS measurements will be discussed by comparing the data with what is obtained from ACS using McCumber relation and also via comparison with direct small signal gain measurements in different axis.

So far we have shown graphs of ECS (λ) at selected temperatures (Figs. 4–6), but it is also quite helpful to look at the same data from a different perspective, by plotting ECS (T) at selected wavelengths. For that purpose, Fig. 7 shows the measured variation of ECS with temperature at selected wavelengths (data acquired by vertically slicing ECS data presented in Figs. 5,6). As expected, as the temperature increases, we see a decrease of ECS value for the peaks of 78 K emission and a slow increase of ECS value for the dips of the 78 K emission. Basically, via increasing phonon energy and increasing rate of electron-phonon coupling, the emission strength is distributed: peaks get wider, dips start to fill, and the ECS spectra gets smoother. If the initial emission peak is very sharp/strong (e.g. 995 nm emission in E//c axis), the slope of decrease

is faster. If the initial strength is moderate (such as the 1019.5 nm line of E//c axis and 1016 nm line of E//a axis), the reduction of ECS value with temperature is slower, which might be advantageous in the design of efficient cryogenic lasers/amplifiers.

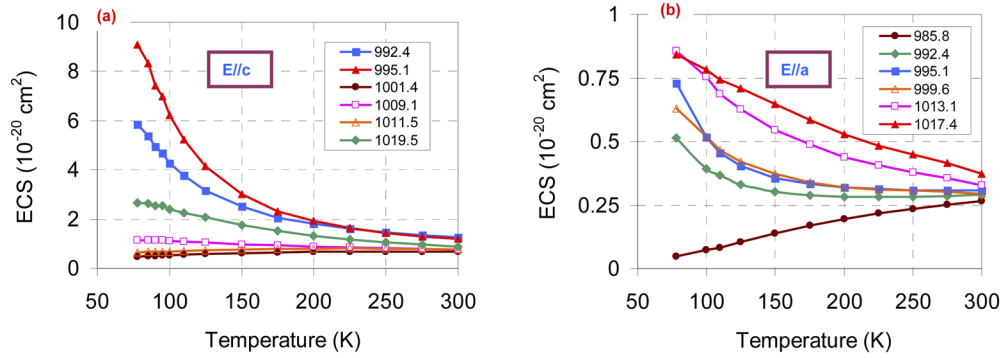


Fig. 7. Variation of measured emission cross section value of Yb:YLF crystal with temperature in the 78–300 K range, at selected wavelengths for (a) E//c and (b) E//a axes.

To our knowledge, the data in Fig. 7, which provides important basic information on laser design, is presented to the first time for Yb:YLF in literature. Hence, we close this section with Table 1, which provides equations for modeling the temperature dependence of emission cross section of Yb:YLF as a function of temperature at selected wavelengths. Note that a relatively complex functional form of:

$$\sigma_e(\lambda, T) = a_0 + a_1 T + a_2 T^2 + a_3 T^3 + a_4 T^4 + a_5 T^5 \quad (8)$$

has been chosen and higher polynomial orders are included only if they are required to obtain a nice fit to the experimentally measured data (a standard Boltzmann distribution formula did not provide a good match to some of the measured trends, and hence, is not preferred). Note, again the coefficients $a_0 - a_5$ in Eq. (8) are wavelength dependent fit parameters.

Table 1. Best fit values of the temperature coefficients in Eq. (8) for the calculation of emission cross section at different temperatures for several representative wavelengths in E//a and E//c axes.

Wavelength (nm) & axis	a_0	a_1 (K^{-1})	a_2 (K^{-2})	a_3 (K^{-3})	a_4 (K^{-4})	a_5 (K^{-5})
992.4 (E//c)	$1.889 \times 10^{+1}$	-2.661×10^{-1}	1.616×10^{-3}	-4.513×10^{-6}	4.768×10^{-9}	-
995.1 (E//c)	$3.423 \times 10^{+1}$	-5.172×10^{-1}	3.189×10^{-3}	-8.932×10^{-6}	9.427×10^{-9}	-
1001.4 (E//c)	2.640×10^{-1}	3.428×10^{-3}	-6.810×10^{-6}	-	-	-
1009.1 (E//c)	1.445×10^0	-3.764×10^{-3}	4.969×10^{-6}	-	-	-
1011.5 (E//c)	4.236×10^{-1}	3.409×10^{-3}	-7.494×10^{-6}	-	-	-
1019.5 (E//c)	4.152×10^0	-2.064×10^{-2}	3.277×10^{-5}	-	-	-
985.8 (E//a)	-8.916×10^{-2}	1.877×10^{-3}	-2.257×10^{-6}	-	-	-
992.4 (E//a)	1.651×10^0	-2.488×10^{-2}	1.701×10^{-4}	-5.139×10^{-7}	5.778×10^{-10}	-
995.1 (E//a)	3.749×10^0	-7.738×10^{-2}	7.110×10^{-4}	-3.280×10^{-6}	7.526×10^{-9}	-6.839×10^{-12}
999.6 (E//a)	1.542×10^0	-1.796×10^{-2}	1.002×10^{-4}	-2.512×10^{-7}	2.356×10^{-10}	-
1013.1 (E//a)	1.553×10^0	-1.156×10^{-2}	4.035×10^{-5}	-5.121×10^{-8}	-	-
1017.4 (E//a)	1.124×10^0	-3.861×10^{-3}	4.594×10^{-6}	-	-	-

5. Emission & absorption cross-check

In this section, we will cross-check our independently obtained emission and absorption cross section results using the McCumber relation. To start with, Fig. 8 shows the calculated ACS curves (obtained from the ECS data presented in the earlier section using Eq. (2)). In general, the observed trend in the curves matches the data in the literature quite well. For a more direct comparison, we could compare the estimated ACS data with the direct ACS measurements that we have taken at 78 K and 300 K.

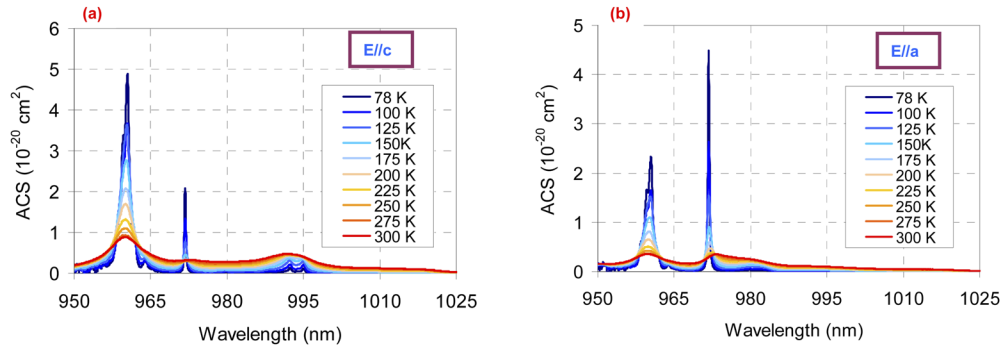


Fig. 8. Calculated variation of absorption cross section with temperature for Yb:YLF crystal in the 78–300 K range for (a) E//c and (b) E//a axes. The ACS data is calculated from the measured emission data using McCumber theory.

For that purpose, Fig. 9 shows the measured ACS data at 78 K and 300 K in both axis along with the curves estimated from ECS (directly measured ACS data is shown with open markers). As a first observation, note that the ACS estimation via McCumber equation is quite noisy and incorrect for wavelengths below 950 nm. Basically, this region is the lower wavelength edge of the ECS data where the SNR ratio in ECS is low, and combined with the limited dynamic range of the spectrometer as well as the exponential nature of McCumber theory, this creates noisy data below 950 nm. Above 950 nm, we observe a relatively good fit to the measured ACS data at 295 K, till one reaches the longer edge of absorption around 1025 nm. In a similar manner, the 78 K curve matches very well to the experimental data in the 950–1000 nm range for the E//a axis and 950–985 nm range for the E//c axis. Essentially, once the measured ACS gets below $0.01 \times 10^{-20} \text{ cm}^2$, a measurement fluctuation of 0.1% in transmitted power creates up to $\pm 5\%$ error in the measured ACS values. As a result, as also discussed in previous literature, the ACS curves obtained from ECS measurements using the McCumber theory provides a better estimate for absorption on longer wavelength side of the absorption curves; whereas, on the short wavelength side, direct absorption measurements provide a much higher accuracy in ACS determination efforts. As an overall observation, we see that the directly measured ACS data and the ACS data calculated from the measured ECS curve fits relatively well to each other in the wavelength range where their harmony is expected, for both 78 K and 295 K measurements.

To cross-check the ACS and ECS curves via McCumber equation at other temperatures, we have used the measured variation of absorption data at selected temperatures (presented earlier in Fig. 3). Figure 10 shows the experimentally measured variation of ACS (open markers) with the McCumber theory estimate based on ECS measurements (solid curves). It is clear that, a relatively good fit exists between the experimentally measured and calculated values, which provide a further sanity check for the earlier measured ECS data.

We would like to finalize this subsection with Fig. 11, which shows the calculated variation of Yb:YLF absorption cross section with temperature on the long wavelength side of absorption, between 975 nm and 1050 nm. The graph is in logarithmic scale, as the absorption in this longer

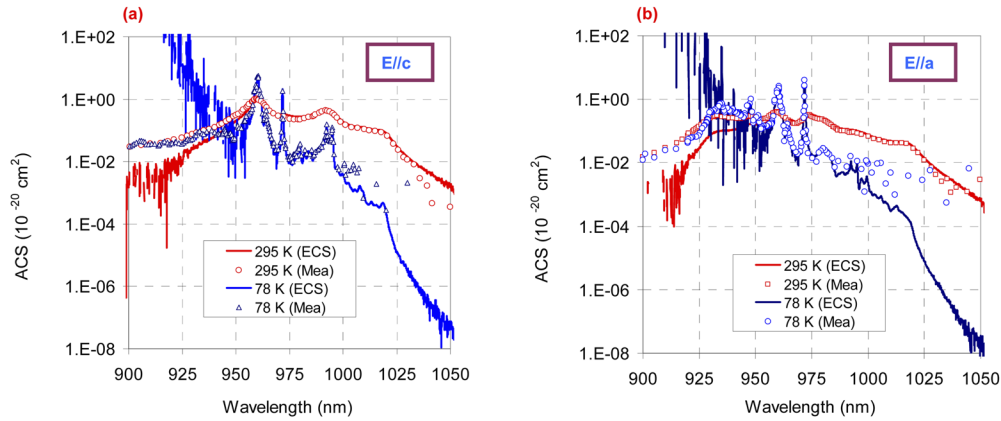


Fig. 9. Comparison of measured and calculated absorption cross section spectra of Yb:YLF for (a) E//c and (b) E//a axes at temperatures of 78 and 295 K. The calculated ACS data is obtained from the measured emission data using McCumber theory.

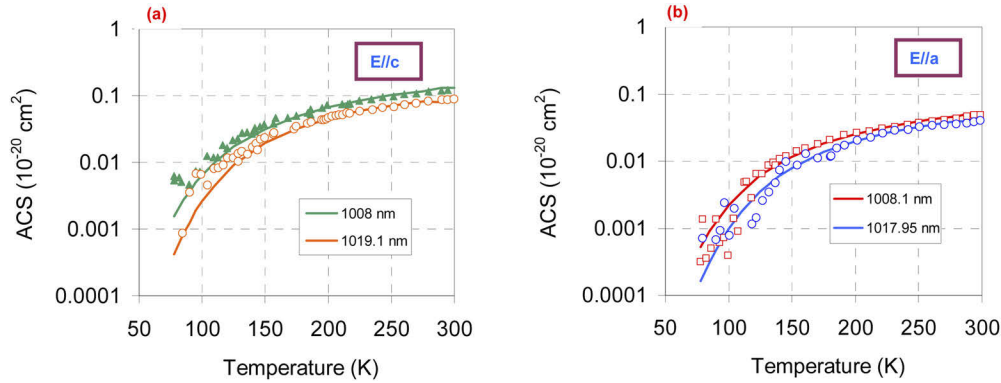


Fig. 10. Comparison of measured (markers) and calculated (solid line) variation of absorption cross section of Yb:YLF with temperature for (a) E//c and (b) E//a axes at selected wavelengths. The calculated ACS data is obtained from the measured emission data using McCumber theory.

end reduces sharply with temperature, and is ignorable for many applications. On the other hand, the solid-state optical refrigerating studies with Yb:YLF [32–38], that is based on anti-Stokes emission of Yb:YLF crystals, ideally needs to achieve absorption at the longer edge (optimum pump wavelength is around ~ 1020 nm) [69]. Moreover, absorption in this region, which overlaps with the regular lasing region of Yb:YLF, appear as self-absorption losses in laser cavities, and should be included in laser modelling. Figure 12 provides the same information from other perspective, and shows the variation of ACS with temperature at several selected wavelengths. If we investigate the data, in terms of their strength near the main lasing bands, we see that the absorption around the 995 peak of Yb:YLF is strong even at 78 K (2 cm of 1% Yb-doped YLF absorbs around 30%), and the laser is 3-level even at cryogenic temperatures (see also the Boltzmann occupancy percentages presented in Fig. 2(e)). At the 1019.5 nm transition of E//c axis and the 1016 nm transition of E//a axis, the ACS curves are more than two order of magnitude weaker at 78 K, enabling almost 4-level lasing at cryogenic temperatures in these transitions. Note that, our measurements for the 1020 nm E//c axis absorption of Yb:YLF matches quite well with the earlier curve reported in [70].

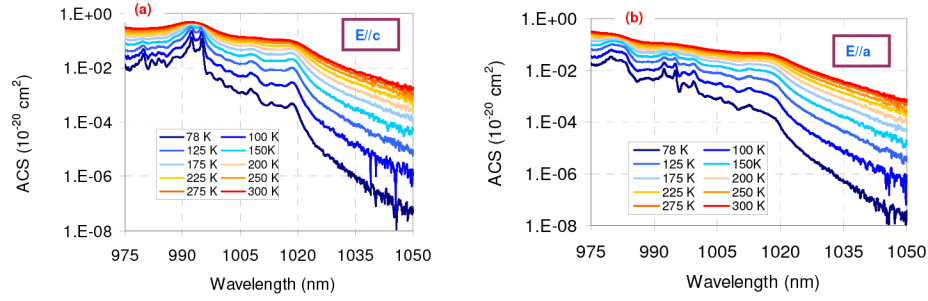


Fig. 11. Calculated variation of Yb:YLF absorption cross section with temperature in logarithmic scale for wavelengths above 975 nm. The ACS data is shown for (a) E//c and (b) E//a axes of Yb:YLF, respectively. The ACS data is calculated from the measured emission data using McCumber theory.

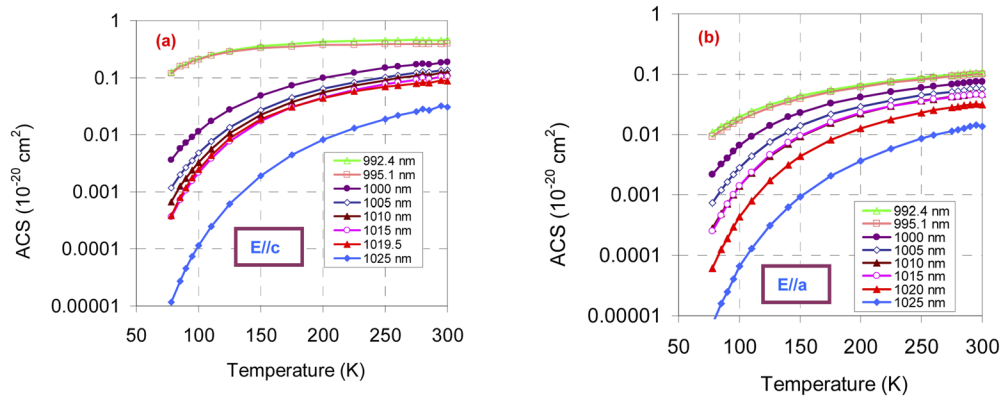


Fig. 12. Calculated variation of absorption cross section of Yb:YLF crystal with temperature in the 78–300 K range, at selected wavelengths for (a) E//c and (b) E//a axes. The ACS data is calculated from the measured emission data using McCumber theory.

To our knowledge, it is hard to find qualitative information in literature on variation of Yb:YLF ACS with temperature. Hence, as we did earlier with ECS data, we will close this section with Table 2, which provides equations for modeling the temperature dependence of absorption cross section of Yb:YLF as a function of temperature at selected wavelengths. Note that a similar functional form of:

$$\sigma_a(\lambda, T) = b_0 + b_1 T + b_2 T^2 + b_3 T^3 + b_4 T^4 + b_5 T^5 + b_6 T^6 \quad (9)$$

has been chosen where the coefficients $b_0 - b_6$ in Eq. (9) are wavelength dependent fit parameters.

Table 2. Best fit values of temperature coefficients for the calculation of absorption cross section at different temperatures for several representative wavelengths in E//a and E//c axes.

Wavelength (nm) & axis	b_0	b_1 (K^{-1})	b_2 (K^{-2})	b_3 (K^{-3})	b_4 (K^{-4})	b_5 (K^{-5})	b_6 (K^{-6})
992.4 (E//c)	-3.905×10^{-1}	8.825×10^{-3}	-3.077×10^{-5}	3.63×10^{-8}	-	-	-
995.1 (E//c)	-5.558×10^{-1}	1.315×10^{-2}	-6.886×10^{-5}	1.603×10^{-7}	-1.383×10^{-10}	-	-
1000 (E//c)	2.937×10^{-2}	-1.037×10^{-3}	1.036×10^{-5}	-1.710×10^{-8}	-	-	-
1005 (E//c)	-9.480×10^{-2}	4.267×10^{-3}	-7.629×10^{-5}	6.754×10^{-7}	-3.007×10^{-9}	6.729×10^{-12}	-6.051×10^{-15}
1010 (E//c)	-7.102×10^{-2}	3.353×10^{-3}	-6.207×10^{-5}	5.605×10^{-7}	-2.528×10^{-9}	5.737×10^{-12}	-5.241×10^{-15}
1015 (E//c)	-5.152×10^{-2}	2.357×10^{-3}	-4.194×10^{-5}	3.590×10^{-7}	-1.504×10^{-9}	3.164×10^{-12}	-2.698×10^{-15}
1019.5 (E//c)	-1.388×10^{-2}	9.881×10^{-4}	-2.307×10^{-5}	2.326×10^{-7}	-1.052×10^{-9}	2.291×10^{-12}	-1.982×10^{-15}
992.4 (E//a)	-2.101×10^{-2}	3.519×10^{-4}	7.949×10^{-7}	-1.722×10^{-9}	-	-	-
995.1 (E//a)	-1.422×10^{-2}	1.942×10^{-4}	1.592×10^{-6}	-3.179×10^{-9}	-	-	-
1000 (E//a)	1.241×10^{-2}	-5.302×10^{-4}	6.473×10^{-6}	-1.925×10^{-8}	1.987×10^{-11}	-	-
1005 (E//a)	-4.568×10^{-2}	2.111×10^{-3}	-3.921×10^{-5}	3.639×10^{-7}	-1.703×10^{-9}	3.971×10^{-12}	-3.677×10^{-15}
1010 (E//a)	-7.331×10^{-2}	3.144×10^{-3}	-5.349×10^{-5}	4.550×10^{-7}	-2.002×10^{-9}	4.451×10^{-12}	-3.968×10^{-15}
1015 (E//a)	-6.297×10^{-2}	2.776×10^{-3}	-4.851×10^{-5}	4.215×10^{-7}	-1.880×10^{-9}	4.219×10^{-12}	-3.789×10^{-15}
1020 (E//a)	-5.676×10^{-2}	2.379×10^{-3}	-3.940×10^{-5}	3.265×10^{-7}	-1.420×10^{-9}	3.166×10^{-12}	-2.860×10^{-15}

6. Gain cross-section calculations

In this subsection, we would like to present calculated gain cross section (GCS) curves for Yb:YLF. Figure 13, which shows the variation of GCS spectra with temperature for both axis for an assumed inversion level of 25%, could be used to initiate a discussion. As we have already discussed while presenting the ECS results, the 1016 nm emission band of E//a axis provides a bandwidth of around 10 nm, which is already sufficiently broad to tolerate sub-150-fs level pulses either via mode-locking or via amplification. Note that the 1016 nm band is not only broad, but it also possesses a relatively flat gain profile, which minimizes gain narrowing effects in amplifiers [27]. If the whole available gain bandwidth of E//a axis could be used, for example in a Kerr-lens mode-locked cryogenic Yb:YLF laser, there is potential to generate sub-100-fs pulses. In contrast, the gain in E//c axis of Yb:YLF is much higher, at the expense of reduced bandwidth. As an example, the 1019.5 nm emission band, which has around 2–3-fold higher gain than the 1016 nm band of E//a axis, owns a FWHM of ~4 nm, but this could already support sub-300-fs pulses.

As we can see, the 992.5 and 995 nm peaks of Yb:YLF is quite narrow and has very high gain at 78 K. Considering the additional advantage of lower quantum defect (995 nm laser pumped at 960 nm), this line becomes very attractive for cw lasing [25], cw amplification [71], or Q-switched lasing with ns-level pulses [62]. One important point to underline here is, in our earlier work, we have seen that, under thermal load, the average temperature of Yb:YLF crystal increases around 0.1–0.2 K per 1 W of absorbed power [30]. Hence, as mentioned earlier, under typical cryogenic laser operation, the average temperature of the Yb:YLF crystal is typically in the 125–150 K range (depending on absorbed pump power, pump spot size, etc.). Hence, it is important to investigate the gain spectra of Yb:YLF in greater detail at slightly elevated temperatures. For that, Fig. 14 shows the calculated gain of Yb:YLF at a temperature of 125 K, for inversion levels between 0 and 100%. Note that, at this temperature, the gain spectra of Yb:YLF gets much more smoother, at the expense of reduced strength. It is interesting to see that, at large inversion levels beyond 75%, the zero-phonon line around 971.7 nm also shows the

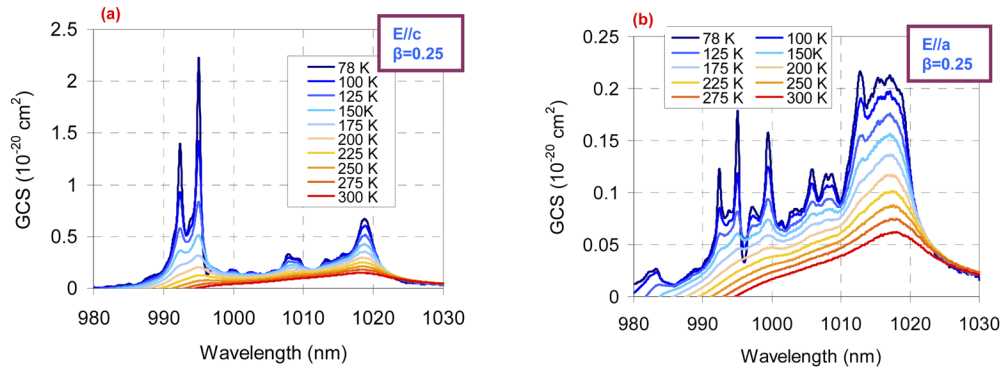


Fig. 13. Calculated variation of Yb:YLF gain cross section (GCS) with temperature for an inversion level of 0.25, for (a) E//c and (b) E//a axes.

potential of lasing for the E//a axis: ideally a 960 nm pumped 971.7 nm cryogenic Yb:YLF laser will work with a quantum defect of only around 1.2%. As another observation, note that, even the 993.5–995 nm transitions are much smoother and at these temperature (~ 125 K), it also seems to have the potential to support sub-500-fs long pulses upon mode-locking or amplification.

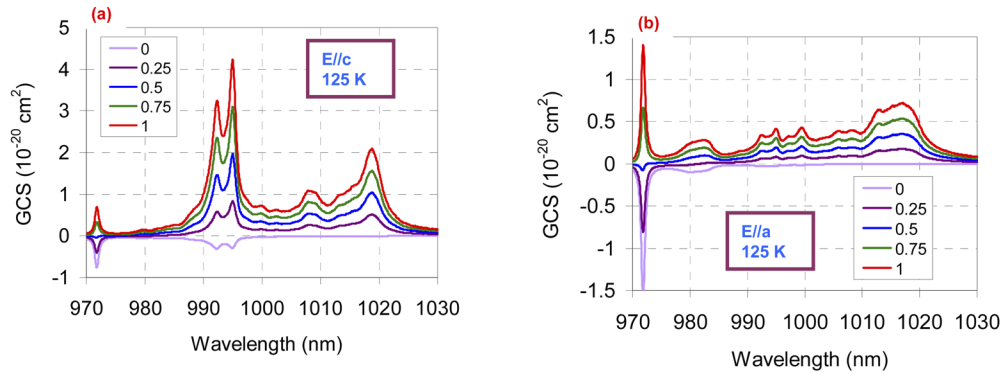


Fig. 14. Calculated variation of Yb:YLF gain cross section (GCS) with inversion at a temperature of 125 K, for (a) E//c and (b) E//a axes.

7. Small signal gain measurements

In this final section, we would like to present direct gain measurement results of Yb:YLF and compare it with the estimates of the gain cross section (GCS) that is presented in the previous section. This provides another alternative approach to investigate the error bars in the earlier emission measurements. To start with, Fig. 15 shows the measured gain spectra of Yb:YLF at (a) 78 K and (b) 295 K along with the calculated GCS profiles at the same temperatures, for an inversion level of 75%. This inversion level is close to the estimated inversion amount in the first few millimeters of the crystal along its length, which then decreases as the beam propagates deeper inside the gain medium due to the lower amount of absorption. The small Cr:LiSAF beam (1.3 mm) also passes through the center of the larger pump spot (3.2 mm), and observes a sweet spot in terms of gain.

When we look at the measured gain profile at 78 K, we first notice that the measured gain in E//c axis is much higher than the gain in E//a axis, which confirms our estimates based on

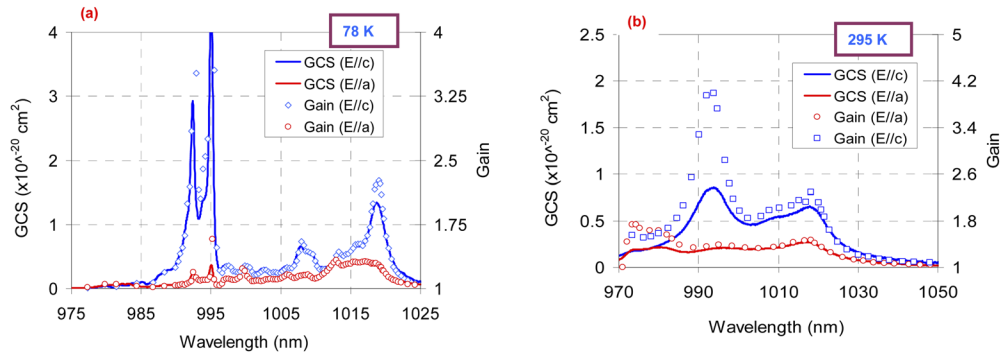


Fig. 15. Comparison of measured variation of small single gain with calculated gain cross section spectra in Yb:YLF for E//c and E//a axes, at temperatures of (a) 78 K and (b) 295 K. The data is taken using a 2 cm long 1% Yb-doped YLF sample at an incident pump energy of 0.5 J and 4 J for the 78 K and 295 K, case respectively. An inversion level of 75% was used in GCS calculation (this is the estimated average inversion level in the first few millimeters of the crystal). An average inversion of around 50% and 20% is estimated through the whole length of the crystal for the 78 K and 300 K cases, respectively.

earlier spectroscopic measurements. Moreover, the measured gain spectra match relatively well to the estimated GCS profile for both polarizations, again confirming the flatness of the spectral response of the measurement system. Note that for the E//c case, the measured gain is slightly higher around the 1019.5 nm peak than what the GCS curve estimates.

We have also measured a single pass gain above 50 near 995 nm, a much higher value than the GCS curve predicts. This data point is not shown in Fig. 15 on purpose (which would otherwise scale down all the other data), but can be observed in Fig. 16, where we plot variation of measured small single gain with temperature at selected wavelengths for both axes. We believe the discrepancy between the measured and estimated gain around the 995 nm peak is again potentially due to the limited resolution of our emission measurement spectrometer. A very high gain (43-dB gain in 14 passes) is also reported recently in a cw amplifier employing the 995 nm line of Yb:YLF (2.6 mW cw signal is amplified to 40 W level), which confirms the strength and sharpness of this line at cryogenic temperatures [71].

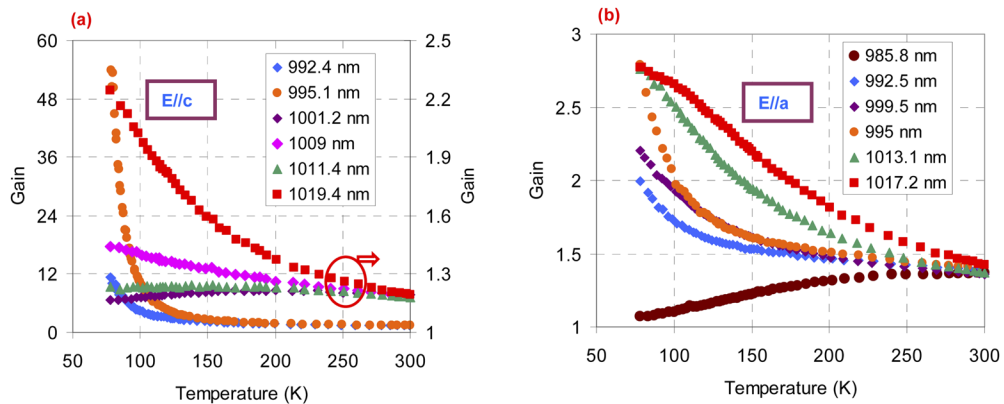


Fig. 16. Measured variation of small single gain with temperature in Yb:YLF for (a) E//c and (b) E//a axes. The data is taken using a 2 cm long 1% Yb-doped YLF sample at an incident pump energy of 0.4 J and 2 J for the E//c and E//a axes, respectively.

It is also interesting to see the sharp decrease of gain, especially for the 995 nm transition: the measured gain already decreased from a value of 50 to around 10 and later to 4 as the temperature increased from 78 K to 100 K and 125 K, respectively. It is important to note that, the measured decrease in gain with temperature involves coupling of many effects: (i) decreasing ECS with temperature, (ii) increasing absorption at seed wavelength with temperature (increasing self-absorption losses), (iii) decreasing absorption at pump wavelength, (iv) increasing fluorescence lifetime with temperature due to increasing role of radiation trapping. We have recently shown that the strong temperature dependence of the 995 nm transition could be used to accurately estimate temperature of Yb:YLF crystal with sub-1-K sensitivity [30].

In closing we would like to briefly discuss Fig. 15(b), in which we observe a mismatch between the measured gain spectra and the calculated GCS curve at room temperature. Note that above 1015 nm the results agree very well, and this is the region where the absorption band does not really overlap with the emission band, and self-absorption effects are minimal. On the other hand, we see that, despite the care taken to minimize self-absorption effects in our ECS measurements, the estimated gain profile does not match the measured gain especially below 1000 nm. Hence, as discussed in literature, the best way to get the correct ECS curve at elevated temperatures is usage of absorption data along with the McCumber theory. Of course, this approach has its own problems/issues, especially in estimating the ECS data at the longer wavelengths. Another approach would be usage of samples with Yb-doping levels below 0.1% or lower; however, the SNR ratio might be an issue at these low doping levels. In our work here, our focus was on cryogenic temperatures (78–150 K), in which the absorption and emission bands do not overlap as much due to the lower phonon energies: as a result, the measured ECS curves do not suffer from radiation-trapping errors as much (as confirmed in Fig. 15(a)). On the other hand, the measurement in Fig. 15(b) shows that, the ECS and GCS curves presented in this work at elevated temperatures might be showing lower values at shorter wavelength region of the spectrum due to ECS/ACS overlap.

8. Conclusions

In conclusion, we have systematically studied temperature dependence of absorption, emission and gain in Yb:YLF in the 78–300 K range. Combining all three in a single study enabled comparison of independently taken experimental results with each other and helped us pinpoint possible error sources. To our knowledge, direct measurements of polarization, wavelength and temperature dependence of small signal gain in Yb:YLF is presented to the first time in this study. We further provided simple analytic formulas for the measured temperature dependence of absorption and emission cross section. We have seen that, the E//a axis of Yb:YLF shows broad gain bandwidth at the expense of lower gain, whereas the E//c axis combines moderate gain bandwidth with high gain. The spectroscopic results show that, future generation of cryogenic Yb:YLF systems has the potential to combine sub-250-fs pulse duration with kW level average powers.

Funding. European Commission (609920).

Acknowledgements. The authors acknowledge support from previous group members L. E. Zapata, K. Zapata for establishing the indium-bonding technology for YLF at CFEL-DESY. UD acknowledges support from BAGEP Award of the Bilim Akademisi. We also thank the anonymous reviewers for their constructive suggestions.

Disclosures. The authors declare no conflicts of interest.

References

1. J. Schulte, T. Sartorius, J. Weitenberg, A. Vernaleken, and P. Russbueldt, "Nonlinear pulse compression in a multi-pass cell," *Opt. Lett.* **41**(19), 4511–4514 (2016).
2. H. Fattahi, H. G. Barros, M. Gorjan, T. Nubbemeyer, B. Alsaif, C. Y. Teisset, M. Schultze, S. Prinz, M. Haefner, M. Ueffing, A. Alismail, L. Vamos, A. Schwarz, O. Pronin, J. Brons, X. T. Geng, G. Arisholm, M. Ciappina, V. S.

- Yakovlev, D. E. Kim, A. M. Azzeer, N. Karpowicz, D. Sutter, Z. Major, T. Metzger, and F. Krausz, "Third-generation femtosecond technology," *Optica* **1**(1), 45–63 (2014).
3. G. M. Rossi, R. E. Mainz, Y. D. Yang, F. Scheiba, M. A. Silva-Toledo, S. H. Chia, P. D. Keathley, S. B. Fang, O. D. Muecke, C. Manzoni, G. Cerullo, G. Cirmi, and F. X. Kaertner, "Sub-cycle millijoule-level parametric waveform synthesizer for attosecond science," *Nat. Photonics* **14**(10), 629–635 (2020).
 4. D. F. Zhang, A. Fallahi, M. Hemmer, X. J. Wu, M. Fakhari, Y. Hua, H. Cankaya, A. L. Calendron, L. E. Zapata, N. H. Matlis, and F. X. Kartner, "Segmented terahertz electron accelerator and manipulator (STEAM)," *Nat. Photonics* **12**(6), 336–342 (2018).
 5. A. Giesen, H. Hugel, A. Voss, K. Wittig, U. Brauch, and H. OPOWER, "Scalable concept for diode-pumped high-power solid-state lasers," *Appl. Phys. B: Lasers Opt.* **58**(5), 365–372 (1994).
 6. C. J. Saraceno, "Mode-locked thin-disk lasers and their potential application for high-power terahertz generation," *J. Opt.* **20**(4), 044010 (2018).
 7. A. Giesen and J. Speiser, "Fifteen years of work on thin-disk lasers: Results and scaling laws," *IEEE J. Sel. Top. Quantum Electron.* **13**(3), 598–609 (2007).
 8. J. Brons, V. Pervak, D. Bauer, D. Sutter, O. Pronin, and F. Krausz, "Powerful 100-fs-scale Kerr-lens mode-locked thin-disk oscillator," *Opt. Lett.* **41**(15), 3567–3570 (2016).
 9. T. Nubbemeyer, M. Kaumanns, M. Ueffing, M. Gorjan, A. Alismail, H. Fattahi, J. Brons, O. Pronin, H. G. Barros, Z. Major, T. Metzger, D. Sutter, and F. Krausz, "1 kW, 200 mJ picosecond thin-disk laser system," *Opt. Lett.* **42**(7), 1381–1384 (2017).
 10. M. Eichhorn, "Quasi-three-level solid-state lasers in the near and mid infrared based on trivalent rare earth ions," *Appl. Phys. B: Lasers Opt.* **93**(2-3), 269–316 (2008).
 11. J. Fischer, A. C. Heinrich, S. Maier, J. Jungwirth, D. Brida, and A. Leitenstorfer, "615 fs pulses with 17 mJ energy generated by an Yb:thin-disk amplifier at 3 kHz repetition rate," *Opt. Lett.* **41**(2), 246–249 (2016).
 12. J. Kawanaka, H. Nishioka, N. Inoue, and K. Ueda, "Tunable continuous-wave Yb : YLF laser operation with a diode-pumped chirped-pulse amplification system," *Appl. Opt.* **40**(21), 3542–3546 (2001).
 13. J. Kawanaka, S. Tokita, H. Nishioka, M. Fujita, T. Kawashima, T. Yanagitani, K. Ueda, and Y. Izawa, "Cryogenically-cooled active-mirror oscillator with Yb-doped material for inertial fusion energy driver," in *Pacific Rim Conference on Lasers & Electro-Optics* (IEEE, Tokyo, Japan, 2005).
 14. K. Beil, S. T. Friedrich-Thornton, C. Kränkel, K. Petermann, D. Parisi, M. Tonelli, and G. Huber, "New thin disk laser materials: Yb:ScYLO and Yb:YLF," in *Conference on Lasers and Electro-Optics Europe* (IEEE, Munich, Germany, 2011).
 15. M. Vannini, G. Toci, D. Alderighi, D. Parisi, F. Cornacchia, and M. Tonelli, "High efficiency room temperature laser emission in heavily doped Yb : YLF," *Opt. Express* **15**(13), 7994–8002 (2007).
 16. D. Alderighi, A. Pirri, G. Toci, and M. Vannini, "Tunability enhancement of Yb:YLF based laser," *Opt. Express* **18**(3), 2236–2241 (2010).
 17. J. Kawanaka, K. Yamakawa, H. Nishioka, and K. Ueda, "Improved high-field laser characteristics of a diode-pumped Yb:LiYF₄ crystal at low temperature," *Opt. Express* **10**(10), 455–460 (2002).
 18. N. Coluccelli, G. Galzerano, L. Bonelli, A. Di Lieto, M. Tonelli, and P. Laporta, "Diode-pumped passively mode-locked Yb:YLF laser," *Opt. Express* **16**(5), 2922–2927 (2008).
 19. F. Pirzio, L. Fregnani, A. Volpi, A. Di Lieto, M. Tonelli, and A. Agnesi, "87 fs pulse generation in a diode-pumped semiconductor saturable absorber mirror mode-locked Yb:YLF laser," *Appl. Opt.* **55**(16), 4414–4417 (2016).
 20. W. Bolanos, F. Starecki, A. Braud, J. L. Doualan, R. Moncorge, and P. Camy, "2.8 W end-pumped Yb³⁺:LiYF₄ waveguide laser," *Opt. Lett.* **38**(24), 5377–5380 (2013).
 21. A. Bensalah, Y. Guyot, A. Brenier, H. Sato, T. Fukuda, and G. Boulon, "Spectroscopic properties of Yb³⁺: LuLiF₄ crystal grown by the Czochralski method for laser applications and evaluation of quenching processes: a comparison with Yb³⁺: YLiF₄," *J. Alloys Compd.* **380**(1-2), 15–26 (2004).
 22. J. Kawanaka, S. Tokita, H. Nishioka, M. Fujita, K. Yamakawa, K. Ueda, and Y. Izawa, "Dramatically improved laser characteristics of diode-pumped Yb-doped materials at low temperature," *Laser Phys.* **15**, 1306–1312 (2005).
 23. D. Rand, D. Miller, D. J. Ripin, and T. Y. Fan, "Cryogenic Yb³⁺-doped materials for pulsed solid-state laser applications [Invited]," *Opt. Mater. Express* **1**(3), 434–450 (2011).
 24. R. L. Aggarwal, D. J. Ripin, J. R. Ochoa, and T. Y. Fan, "Measurement of thermo-optic properties of Y₃Al₅O₁₂, Lu₃Al₅O₁₂, YAlO₃, LiYF₄, LiLuF₄, BaY₂F₈, KGd(WO₄)₂, and KY(WO₄)₂ laser crystals in the 80-300 K temperature range," *J. Appl. Phys.* **98**(10), 103514 (2005).
 25. L. E. Zapata, D. J. Ripin, and T. Y. Fan, "Power scaling of cryogenic Yb:LiYF₄ lasers," *Opt. Lett.* **35**(11), 1854–1856 (2010).
 26. U. Demirbas, H. Cankaya, J. Thesinga, F. X. Kartner, and M. Pergament, "Efficient, diode-pumped, high-power (>300W) cryogenic Yb:YLF laser with broad-tunability (995-1020.5 nm): investigation of E//a-axis for lasing," *Opt. Express* **27**(25), 36562–36579 (2019).
 27. U. Demirbas, H. Cankaya, Y. Hua, J. Thesinga, M. Pergament, and F. X. Kaertner, "20-mJ, sub-ps pulses at up to 70 W average power from a cryogenic Yb:YLF regenerative amplifier," *Opt. Express* **28**(2), 2466–2479 (2020).
 28. D. E. Miller, L. E. Zapata, D. J. Ripin, and T. Y. Fan, "Sub-picosecond pulses at 100 W average power from a Yb:YLF chirped-pulse amplification system," *Opt. Lett.* **37**(13), 2700–2702 (2012).

29. U. Demirbas, J. Thesinga, H. Cankaya, M. Kellert, F. X. Kartner, and M. Pergament, "High-power passively mode-locked cryogenic Yb:YLF laser," *Opt. Lett.* **45**(7), 2050–2053 (2020).
30. U. Demirbas, J. Thesinga, M. Kellert, F. X. Kartner, and M. Pergament, "Comparison of different in situ optical temperature probing techniques for cryogenic Yb:YLF," *Opt. Mater. Express* **10**(12), 3403–3413 (2020).
31. U. Demirbas, H. Cankaya, J. Thesinga, F. X. Kartner, and M. Pergament, "Power and energy scaling of rod-type cryogenic Yb:YLF regenerative amplifiers," *J. Opt. Soc. Am. B* **37**(6), 1865–1877 (2020).
32. S. Melgaard, "Cryogenic optical refrigeration: Laser cooling of solids below 123 K," (University of New Mexico, 2013).
33. S. D. Melgaard, A. R. Albrecht, M. P. Hehlen, and M. Sheik-Bahae, "Solid-state optical refrigeration to sub-100 Kelvin regime," *Sci. Rep.* **6**(1), 20380 (2016).
34. D. V. Seletskiy, S. D. Melgaard, S. Bigotta, A. Di Lieto, M. Tonelli, and M. Sheik-Bahae, "Laser cooling of solids to cryogenic temperatures," *Nat. Photonics* **4**(3), 161–164 (2010).
35. S. Melgaard, D. Seletskiy, V. Polyak, Y. Asmerom, and M. Sheik-Bahae, "Identification of parasitic losses in Yb:YLF and prospects for optical refrigeration down to 80 K," *Opt. Express* **22**(7), 7756–7764 (2014).
36. A. Pant, X. J. Xia, E. J. Davis, and P. J. Pauzauskie, "Solid-state laser refrigeration of a composite semiconductor Yb:YLiF₄ optomechanical resonator," *Nat. Commun.* **11**(1), 3235 (2020).
37. A. Di Lieto, A. Sottile, A. Volpi, Z. H. Zhang, D. V. Seletskiy, and M. Tonelli, "Influence of other rare earth ions on the optical refrigeration efficiency in Yb:YLF crystals," *Opt. Express* **22**(23), 28572–28583 (2014).
38. A. Volpi, A. Di Lieto, and M. Tonelli, "Novel approach for solid state cryocoolers," *Opt. Express* **23**(7), 8216–8226 (2015).
39. U. Demirbas and I. Baali, "Power and efficiency scaling of diode pumped Cr: LiSAF lasers: 770–1110 nm tuning range and frequency doubling to 387–463 nm," *Opt. Lett.* **40**(20), 4615–4618 (2015).
40. U. Demirbas, "Cr: colquiriite lasers: current status and challenges for further progress," *Prog. Quantum Electron.* **68**, 100227 (2019).
41. U. Demirbas, M. Schmalz, B. Sumpf, G. Erbert, G. S. Petrich, L. A. Kolodziejski, J. G. Fujimoto, F. X. Kartner, and A. Leitenstorfer, "Femtosecond Cr:LiSAF and Cr:LiCAF lasers pumped by tapered diode lasers," *Opt. Express* **19**(21), 20444–20461 (2011).
42. P. F. Moulton, "Spectroscopic and laser characteristics of Ti:Al₂O₃," *J. Opt. Soc. Am. B* **3**(1), 125–133 (1986).
43. D. Pugh-Thomas, B. M. Walsh, and M. C. Gupta, "Spectroscopy of BeAl₂O₄:Cr³⁺ with application to high-temperature sensing," *Appl. Opt.* **49**(15), 2891–2897 (2010).
44. D. E. McCumber, "Theory of phonon-terminated optical masers," *Phys. Rev.* **134**(2A), A299–A306 (1964).
45. D. E. McCumber, "Einstein relations connecting broadband emission and absorption spectra," *Phys. Rev.* **136**(4A), A954–A957 (1964).
46. M. L. Shand, J. C. Walling, and H. P. Jenssen, "Ground-state absorption in the lasing wavelength region of Alexandrite - theory and experiment," *IEEE J. Quantum Electron.* **18**(2), 167–169 (1982).
47. J. Korner, M. Kruger, J. Reiter, A. Munzer, J. Hein, and M. C. Kaluza, "Temperature dependent spectroscopic study of Yb³⁺-doped KG(WO₄)₂, KY(WO₄)₂, YAlO₃ and YLiF₄ for laser applications," *Opt. Mater. Express* **10**(10), 2425–2438 (2020).
48. L. D. DeLoach, S. A. Payne, L. L. Chase, L. K. Smith, W. L. Kway, and W. F. Krupke, "Evaluation of absorption and emission properties of yb doped crystals for laser applications," *IEEE J. Quantum Electron.* **29**(4), 1179–1191 (1993).
49. B. Sumpf, K. H. Hasler, P. Adamiec, F. Bugge, F. Dittmar, J. Fricke, H. Wenzel, M. Zorn, G. Erbert, and G. Trankle, "High-brightness quantum well tapered lasers," *IEEE J. Sel. Top. Quantum Electron.* **15**(3), 1009–1020 (2009).
50. B. Sumpf, P. Adamiec, M. Zorn, H. Wenzel, and G. Erbert, "Nearly diffraction limited tapered lasers at 675 nm with 1 W output power and conversion efficiencies above 30%," *IEEE Photonics Technol. Lett.* **23**(4), 266–268 (2011).
51. U. Demirbas, "Off-surface optic axis birefringent filters for smooth tuning of broadband lasers," *Appl. Opt.* **56**(28), 7815–7825 (2017).
52. U. Demirbas, S. Eggert, and A. Leitenstorfer, "Compact and efficient Cr:LiSAF lasers pumped by one single-spatial-mode diode: a minimal cost approach," *J. Opt. Soc. Am. B* **29**(8), 1894–1903 (2012).
53. H. Burton, C. Debardeleben, W. Amir, and T. A. Planchon, "Temperature dependence of Ti:Sapphire fluorescence spectra for the design of cryogenic cooled Ti:Sapphire CPA laser," *Opt. Express* **25**(6), 6954–6962 (2017).
54. X. Peng and L. Dong, "Temperature dependence of ytterbium-doped fiber amplifiers," *J. Opt. Soc. Am. B* **25**(1), 126–130 (2008).
55. A. Bensalah, Y. Guyot, M. Ito, A. Brenier, H. Sato, T. Fukuda, and G. Boulon, "Growth of Yb³⁺-doped YLiF₄ laser crystal by the Czochralski method. Attempt of Yb³⁺ energy level assignment and estimation of the laser potentiality," *Opt. Mater.* **26**(4), 375–383 (2004).
56. A. Sugiyama, M. Katsurayama, Y. Anzai, and T. Tsuboi, "Spectroscopic properties of Yb doped YLF grown by a vertical Bridgman method," *J. Alloys Compd.* **408–412**, 780–783 (2006).
57. C. A. Morrison and R. P. Leavitt, "Spectroscopic properties of triply ionized lanthanides in transparent host crystals," in *Handbook on the Physics and Chemistry of Rare Earths*, K. A. Gschneidner and L. Eyring, eds. (North-Holland Publishing Company, 1982).
58. H. Ogilvy, M. J. Withford, R. P. Mildren, and J. A. Piper, "Investigation of the pump wavelength influence on pulsed laser pumped Alexandrite lasers," *Appl. Phys. B: Lasers Opt.* **81**(5), 637–644 (2005).

59. T. Y. Fan, D. J. Ripin, R. L. Aggarwal, J. R. Ochoa, B. Chann, M. Tilleman, and J. Spitzberg, "Cryogenic Yb^{3+} -doped solid-state lasers," *IEEE J. Sel. Top. Quantum Electron.* **13**(3), 448–459 (2007).
60. N. P. Barnes and D. J. Gettemy, "Temperature-variation of the refractive-indexes of yttrium lithium-fluoride," *J. Opt. Soc. Am.* **70**(10), 1244–1247 (1980).
61. U. Demirbas, J. Thesinga, M. Kellert, M. Pergament, and F. X. Kärtner, "Temperature and doping dependence of fluorescence lifetime in Yb:YLF (role of impurities)," *Optical Materials* (2021, in press).
62. N. Ter-Gabrielan, V. Fromzel, T. Sanamyan, and M. Dubinskii, "Highly-efficient Q-switched Yb: YLF laser at 995 nm with a second harmonic conversion," *Opt. Mater. Express* **7**(7), 2396–2403 (2017).
63. N. Uehara, K. Ueda, and Y. Kubota, "Spectroscopic measurements of a high-concentration Yb^{3+} :LiYF₄ crystal," *Jpn. J. Appl. Phys.* **35**(4B), L499–L501 (1996).
64. G. Boulon, Y. Guyot, M. Ito, A. Bensalah, C. Goutaudier, G. Panczer, and J. C. Gacon, "From optical spectroscopy to a concentration quenching model and a theoretical approach to laser optimization for Yb^{3+} -doped YLiF₄ crystals," *Mol. Phys.* **102**(11-12), 1119–1132 (2004).
65. G. Cittadino, A. Volpi, A. Di Lieto, and M. Tonelli, "Czochnski crystal growth for laser cooling," *Opt. Eng.* **56**(1), 011107 (2016).
66. D. V. Seletskiy, S. D. Melgaard, R. I. Epstein, A. Di Lieto, M. Tonelli, and M. Sheik-Bahae, "Precise determination of minimum achievable temperature for solid-state optical refrigeration," *J. Lumin.* **133**, 5–9 (2013).
67. J. Kawanaka, K. Yamakawa, H. Nishioka, and K. Ueda, "30-mJ, diode-pumped, chirped-pulse Yb : YLF regenerative amplifier," *Opt. Lett.* **28**(21), 2121–2123 (2003).
68. S. Cante and J. I. Mackenzie, "Spectroscopic Characterisation of Yb:LiLuF₄ between (63-293)K," in *Laser Congress 2019 (ASSL, LAC, LS&C)* (OSA, 2019), p. JM5A.4.
69. S. Melgaard, D. Seletskiy, M. Sheik-Bahae, S. Bigotta, A. D. Lieto, M. Tonelli, and R. Epstein, "Spectroscopy of Yb-doped YLF crystals for laser cooling," in *SPIE OPTO, Laser Refrigeration of Solids III* (SPIE, 2010), p. 761407.
70. J. Meng, A. R. Albrecht, A. Gragossian, E. Lee, A. Volpi, M. Ghasemkhani, M. P. Hehlen, R. I. Epstein, and M. Sheik-Bahae, "Realization of an all-solid-state cryocooler using optical refrigeration," in *SPIE Defense + Security Tri-Technology Device Refrigeration (TTDR) III* (SPIE, Orlando, Florida, United States, 2018), p. 761407.
71. J. Manni, D. Harris, and T. Y. Fan, "High-gain (43 dB), high-power (40 W), highly efficient multipass amplifier at 995 nm in Yb:LiYF₄," *Opt. Commun.* **417**, 54–56 (2018).